CRITICAL CURRENTS AND MAGNETIZATION OF SUPERCONDUCTING ALLOYS

Yu. F. BYCHKOV, N. G. VASIL'EV, V. G. VERESHCHAGIN, V. G. ERSHOV, M. T. ZUEV, V. P. KARASIK, G. B. KURGANOV, D. V. PRONKIN, and A. I. RUSINOV

P. N. Lebedev Physics Institute, USSR Academy of Sciences

The dependence of the transverse critical current on external magnetic field strength ($j \perp H$) and temperature of Zr-Nb alloys is investigated in the region $0 < H < H_{c2}$. The results obtained are interpreted on the basis of information regarding the structural state of the alloys and by applying the model of a rigidly pinned vortex lattice in which the proximity effect is taken into account. The complete cycle of the magnetization hysteresis curve is described analytically by applying the Bean critical-state concept to a superconducting alloy with a rigidly pinned fluxoid system, the dependence of critical current on external magnetic field being exponential. Satisfactory agreement between the experimental dependence M(H) and the theoretical calculations is demonstrated for model Zr-20%Nb and Zr-35%Nb alloys at magnetic-field strengths ranging from 0 to 0.5 H_{c2}.

AS has been shown previously[1], the behavior of critical currents in superconducting alloys containing particles of the transition ω phase uniformly distributed over the volume depends on the relation between the linear dimensions of the ω particles d and the core diameter of the Abrikosov vortex 2ξ. When $d < 2\xi$ the superconductivity is destroyed under the action of Lorentz forces, and therefore the critical currents are small. For $d \sim 2\xi$ the peak-effect is observed, and for $d > 2\xi$ the vortex lattice is rigidly pinned and destruction of the superconductivity is due to the achievement of the critical velocity by the superconducting condensate.

It was of interest to learn how general the results obtained are. For this purpose we have studied $j_c(H)$ and M(H) in Zr-Nb alloys rich in Zr, in which, as in Ti-Nb alloys[1], it is possible by varying the temperature and aging time to control the size and concentration of the ω particles. The largest number of measurements have been made on objects containing one type of stabilizing defect vortex—ω particles in a recrystallized matrix[1]. The measurements were made in the apparatus and by the methods described previously[1,8].

1. STRUCTURAL STATE OF THE SAMPLES

In Zr-Nb alloys recrystallized by holding at 800°C and containing 15–35% Nb, the ω phase is formed in the aging process at temperatures of 300–450°C. The decomposition occurs according to the scheme[9]

$$\beta \to \omega + \beta^* \to \alpha + \beta_{Nb},$$
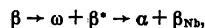
where β^* is the matrix enriched in Nb; α and β_{Nb} are the equilibrium phases; the α phase consists of Zr with a small addition of Nb and has a superconducting transition temperature which does not exceed 1°K; the ω phase contains 8–10% Nb, and has $T_c < 4.2$°K. The phase β_{Nb} in the equilibrium state contains 85% Nb.

In the alloy Zr-20% Nb ω particles with linear dimensions $d \sim 2\xi$ are separated in the recrystallized matrix at 350–450°C in a time of 1–10 hours[2]. As the Nb content is increased to 35%, a noticeable decomposition is observed under the same conditions only after preliminary cold work.

In preparation of the samples the initial material was zirconium and niobium iodides refined by electron-beam melting. The ingots were melted in an arc furnace in a water-cooled copper hearth in an atmosphere of pure argon. From them were machined rods which served as the initial material for preparation of wire and ribbon. After preliminary cleaning of the surface the prepared samples were subjected to annealing in a vacuum of 10^{-5} Torr or better.

An x-ray structural analysis was made with an x-ray diffraction camera with Cu K_α radiation. Information on the samples is summarized briefly in the table.

Sample No.	D, mm	D_0^2/D^2	Annealing at final diameter		Phase composition		
			t, °C	τ, hrs.	β phase	ω phase	α phase
Alloy Zr–20% Nb							
9	0.205	1	—	—	+	—	—
10	0.240	1	350	1	+	+	—
12	0.220	1	350	3	+	+	—
16	0.215	1	350	5	+	+	—
49	0.260	1	450	0,5	+	+	—
29	0.250	1	450	1	+	+	—
63	0.240	1	450	5	+	+	—
Alloy Zr–35% Nb							
26	0.245	1	—	—	+	—	—
60	0.250	1	500	5	+	—	+
44	0.245	1600	450	3	+	—	+
55a	0.730	1600	450	10	+	—	+
556	0.500	1600	450	10	+	—	+
55в	0.260	1600	450	10	+	—	+

Note. Here D_0^2/D^2 is the degree of deformation; D_0 is the sample diameter after recrystallization; D is the final sample diameter.

---

[1] Alloys of the Zr-Nb system containing ω particles in a deformed matrix have been studied previously [2-7]. These studies first demonstrated the effectiveness of ω particles as pinning centers for Abrikosov vortices.

[2] V. A. Vazilkin has used a transmission electron microscope and microdiffraction to obtain a photograph of a portion of a ribbon of Zr-20% Nb alloy previously recrystallized and subjected to aging for one hour at 450°C. ω particles of circular form are clearly visible in the photograph. The average diameter of the particles is 150Å ($2\xi \approx 120$Å).

2. CRITICAL CURRENT MEASUREMENTS AND DISCUSSION

Figure 1 shows a series of curves $j_c(H)$ obtained in samples of Zr-20% Nb alloy subjected to various lengths of aging after preliminary recrystallization. It is evident that in sample No. 9, which was heated after recrystallization, the critical current density rapidly falls with increasing magnetic field. A similar curve was obtained in sample No. 10 (aging temperature 350°C, time of aging τ = 1 hour). With increase of τ to 3 hours (sample No. 12) j_c rises significantly, and a maximum appears in the $j_c(H)$ curve. With further increase of τ the maximum is displaced toward low fields and is converted to a plateau. Increasing the aging temperature to 450°C for τ = 5 hours completely removes the maximum (sample 63).

It is characteristic that in all samples shown in Fig. 1 the upper critical field H_{C2} is the same. According to Ralls et al.,[10] H_{C2} in the Zr-Nb system increases on increase of the Nb content from 20 to 40% with an average rate of about 2 kOe/% Nb. Therefore the constancy of H_{C2} indicates the independence of the matrix composition of these samples on the annealing conditions. It is not excluded that in breakup of the solid solution in the initial Zr-20% Nb alloy in an unchanging β matrix ω particles are formed, surrounded by a zone strongly enriched in Nb.

Figure 2 shows the temperature dependence of the peak-effect in samples 29 and 49, which differ from samples 10 and 12 in the temperature and time of aging (see the table). Figure 2 also demonstrates the temperature dependence $j_c(H)$ of sample 63. The measured values of $j_c(H)$ for samples of Zr-35% Nb alloy are shown in Fig. 3. It can be seen that aging alone after recrystallization (Fig. 3, sample 60) affects the critical currents rather weakly. Cold working alone gives similar results. At the same time, aging carried out after preliminary cold work increases j_c by many times (Fig. 3, sample 44).

The results presented above can be explained by the interaction of Abrikosov vortices with ω particles.

In sample 9 there are no ω particles and the final critical current is due to the presence of dislocations,

crystallite boundaries, impurity clusters, and so forth, remaining after the recrystallization.

In sample 10 the ω phase exists, but as a result of the short aging period the ω particles have linear dimensions d less than the coherence length. Therefore the vortex lattice is not stabilized and the critical currents are low. Increasing the aging period τ leads to an increase of d. When d becomes comparable with the diameter of the vortex core, a maximum appears in the $j_c(H)$ curve (the peak-effect), due to destruction of the induced superconductivity of the ω particles as the result of diffusion of superconducting pairs from the matrix (the proximity effect). Further increase of τ displaces the peak toward low magnetic fields, since the ω particles increase in size and the action of the proximity effect is weakened (the diffusion of pairs occurs to a distance $\xi(T)$).

The process described is similar in many ways to the phenomena observed in the superconducting alloy Ti-22% Nb.[1] The main difference is the nature of the temperature dependence of the critical current in the presence of the peak-effect. In the alloy Zr-20% Nb in
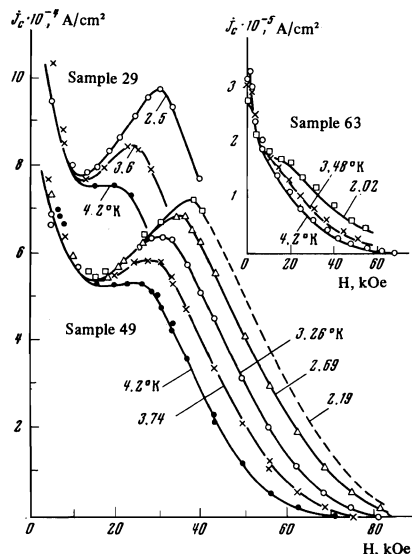
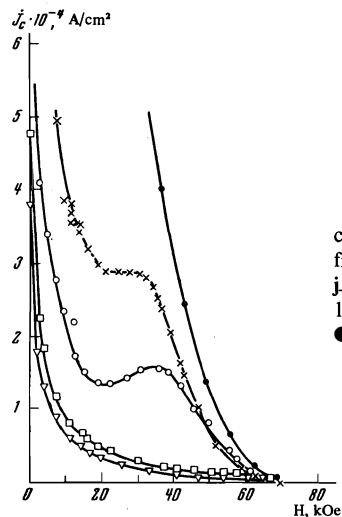FIG. 2. Temperature dependence of the peak effect. Alloy Zr-20% Nb, j⊥H.

FIG. 1. Dependence of critical current density on magnetic field. Alloy Zr-20% Nb, T = 4.2°K, j⊥H. ▽—sample No. 9, □—sample 10, ○—sample 12, ✕—sample 16, ●—sample 63.
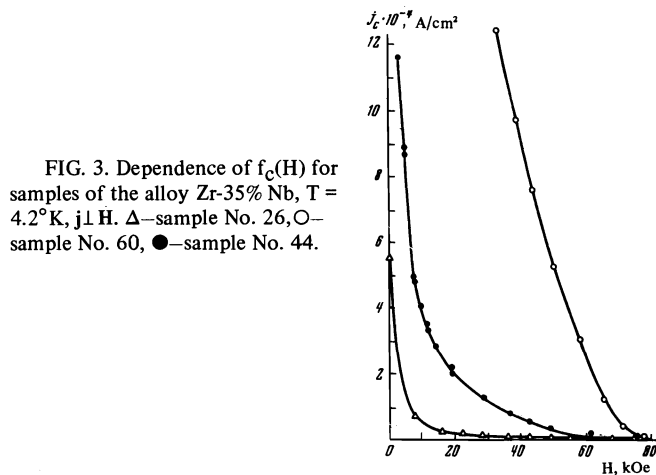
FIG. 3. Dependence of $f_c(H)$ for samples of the alloy Zr-35% Nb, T = 4.2°K, j⊥ H. △—sample No. 26, ○—sample No. 60, ●—sample No. 44.

the region beginning near the minimum of the critical current (see Fig. 2, samples 29 and 49), the critical current does not depend on temperature, while in the alloy Ti-22% Nb the current j_c increases uniformly as the temperature is reduced over the entire region $0 < H < H_{C2}$. Beyond the maximum the temperature dependence of j_c is the same in the two alloys and accurately follows the law[11]

$$j_c(t) = j_c(0)(A - t^2)^2, \qquad (1)$$

where $t = T/T_C$ and A does not depend on H.

In sample No. 63 the ω particles at 4.2°K are in the normal state. On reduction of the temperature they become superconducting in the region $0 < H < H_{C2}^{\omega}(t)$. As a result of this the $j_C(H)$ curves for sample 63 for $T \lesssim 3.5$°K show a special behavior[3].

The difference in behavior of j_C in titanium and zirconium alloys is evidently due to the different kinetics of the ω phase formation. In Ti-22% Nb alloy the diffusion process occurs at a high rate in aging. Therefore Nb leaving the ω particles is distributed practically uniformly in the matrix. In Zr-20% Nb alloy the diffusion rate is substantially lower, and this may lead to formation of a three-phase system. Here the Nb-rich layer adjacent to the ω particles can have a condensation energy greater than in the matrix and can serve as a potential barrier preventing localization of the vortices at the ω particles[13] (T_C rises as the niobium concentration is increased to ~50%). If a barrier exists, then for $H < H_{C2}^{\omega}(t)$ the vortices must be located between the ω particles, and the rise in current (peak-effect) corresponds to penetration of the vortices through the barrier, whose height is reduced as the magnetic field strength is increased[13].

From the results obtained in Zr-35% Nb alloy, it follows that this solid solution has increased stability against breakup in comparison with Zr-20% Nb alloy: breakup becomes appreciable only with the combined action of cold work and subsequent aging, in the course of which α-phase particles are separated (see the table). The critical temperature of the α phase is less than 1°K, and therefore we did not observe the peak effect associated with it.

In order to obtain additional information on the superconducting properties of the ω phase, we prepared and studied samples of the alloy Zr-10% Nb, in which on cooling from the β region a quantity close to 100% of the ω phase is formed with a small amount of the β phase. Measurements of T_c made by the induction method showed that the transition curve has the shape characteristic of single-phase samples (T_c = 4.57°K, ΔT_c = 0.05°K). Apparently the ω particles produced are so small that as a result of the proximity effect the superconducting properties of the ω and β phases are completely averaged and it is impossible to separate them.

To obtain additional information on the superconducting properties of alloys based on zirconium we measured magnetization curves in samples having a rigid vortex lattice.[1,8] The results obtained were compared with the theoretical results.

3. CALCULATION OF THE COMPLETE HYSTERESIS CYCLE

In alloys with a rigid vortex lattice[1,8] the critical current density is related to the magnetic field in the region $0 < H_0 < 0.5\, H_{C2}$ by the relation

$$j_c(H) = j_c(0) \exp(-H/H_{cr}), \qquad (2)$$

where $j_c(0) = j_0$ and H_{cr} are parameters of a given material, determined experimentally.

Use of Bean's concept of a critical state[14] together with Eq. (2) provides the possibility of analytically describing the complete hysteresis cycle.

We will assume that the distribution of magnetization currents in the critical state is given by Eq. (2). Figure 4 shows an idealized magnetization curve of a superconducting alloy. The letters designate the portions of the curve successively traversed. It is evident from this figure that the magnetization in a given field M(H) depends substantially on the previous history of field application.

Physically this is due to the fact that on complete removal of the field ($H_0 = 0$) a large magnetic moment remains frozen in the sample (point e in Fig. 4). The possibility of describing the hysteresis behavior of superconducting alloys in the critical-state model is due to the arbitrariness in choice of the direction of the magnetization currents which appear in Maxwell's equation

$$\text{rot}\, \mathbf{H} = 4\pi c^{-1} \mathbf{j}(H). \qquad (3)$$

We will consider an infinitely long cylinder of radius R placed in a longitudinal external magnetic field $H = H_0$ and in the critical state. Figure 5 gives a qualitative picture of the magnetic field distribution inside the sample as a function of the advance along the magnetization curve. The letters at the right show the part of the M(H) curve to which the distribution H(r) refers.

We will introduce the dimensionless variables:

$$r = \frac{\tilde{r}}{R}, \qquad h = \frac{\tilde{H}}{H_{cr}}, \qquad \gamma = \frac{4\pi j_0 R}{c H_{cr}}, \qquad \mathscr{M} = \frac{4\pi M}{H_{cr}}, \qquad (4)$$

where $\tilde{r}$ and $\tilde{H}$ are the instantaneous values of radius and magnetic field. In these variables Eq. (3) with inclusion of Eq. (2) takes the form

$$-dh/dr = -\gamma e^{-h}. \qquad (5)$$

The minus sign in the right-hand side of Eq. (5) indicates the diamagnetic nature of the induced currents in
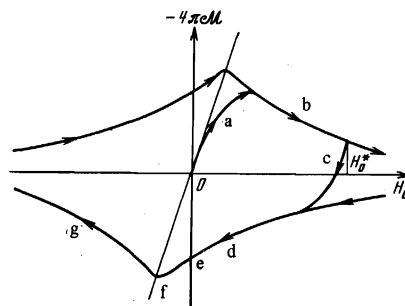

FIG. 4. Idealized magnetization curve of a superconducting alloy. H_0 is the external magnetic field.

---

[3]Goncharov et al. [12] have reported observation of the peak effect on cooling samples of Zr-25% Nb alloy to $T \lesssim 3$°K.
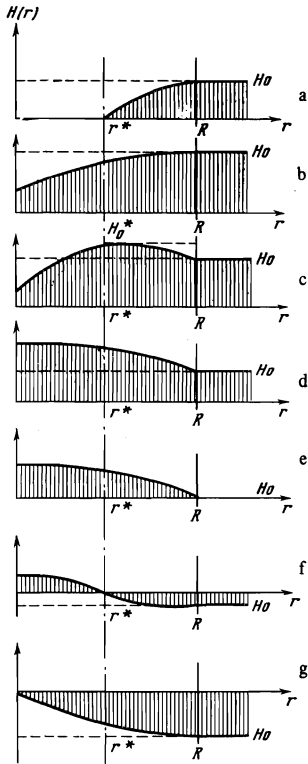
FIG. 5. Distribution of magnetic field inside the sample. R is the sample radius.

the sample. This corresponds to the state a and b in Figs. 4 and 5.

Integration of Eq. (5) has been carried out by Karasik et al.[8]; an expression was obtained which describes the portion of the magnetization curve O-a-b-H_{C2}, and the current and field distributions were given in this region as a function of the radius of the cylinder. Here we will describe the complete hysteresis loop. For this purpose we will now assume that the external field H_0 exceeds the value H_{C2} for the material in hand (here we do not take into account the effect of magnetization currents of surface superconductivity, since the surface-current magnetization does not exceed 10 Oe). A subsequent decrease of the field then leads to appearance on the surface of the sample of induced currents which have the opposite sign relative to the direction of currents in portions a and b. Thus, the state of a sample with a frozen moment can be considered as a paramagnetic state (see Fig. 5, case d). Then the relation between current density and magnetic field has the following form:

$$-dh/dr = \gamma e^{-h}, \quad h > 0. \tag{6}$$

In the positive magnetic field region in the portion d the field inside the sample changes according to a law

$$H(r) = \ln [\, e^h + \gamma(1 - r)\,]. \tag{7}$$

Substituting this solution into the expression for the sample moment

$$-\mathscr{M} = \int_0^1 r^2 \frac{dh}{dr} dr, \tag{8}$$

we finally obtain

$$\mathscr{M}_d = -\frac{3}{2} - \frac{1}{\gamma} e^h + \frac{(e^h + \gamma)^2}{\gamma^2}[\ln(e^h + \gamma) - h], \quad h > 0. \tag{9}$$

In particular, the "frozen" magnetic moment for $H_0 = 0$ is

$$\mathscr{M}_e = -\frac{3}{2} - \frac{1}{\gamma} + \frac{(1 + \gamma)^2}{\gamma^2}\ln(1 + \gamma). \tag{10}$$

On further motion along the magnetization curve to the negative-field region in the portion from e to f, the field H inside the sample changes sign (H < 0) only in a certain near-surface region $r^* \le r \le 1$, while in the central part of the sample it attempts to retain its previous direction (H > 0) for $0 \le r < r^*$ (see Figs. 4 and 5, cases e and f). Thus, in the portion from e to f Eq. (6) has the form

$$-dh/dr = \gamma e^{-|h|}, \quad h < 0. \tag{11}$$

The solution of this equation with allowance for the change of sign of the field H at $r = r^*$ has the following form:

$$H(r) = \begin{cases} -\ln[e^{-h} - \gamma(1 - r)], & r^* \le r \le 1, \; h < 0; \\ \ln[1 + \gamma(r^* - r)], & 0 \le r \le r^*, \; h > 0. \end{cases} \tag{12}$$

Joining the two solutions at the point $r = r^*$ ($h(r^*) = 0$), we find the relation between r^* and h:

$$e^{-h} - 1 = \gamma(1 - r^*). \tag{13}$$

Carrying out the integration in Eq. (8), we eventually obtain an expression for the magnetic moment for negative values of the magnetic field H_0 in the vicinity of f:

$$\mathscr{M}_f = \frac{1}{2} - \frac{1}{\gamma} - 3(r^*)^2 + r^* + \frac{(1 + \gamma r^*)^2}{\gamma^2}\ln(1 + \gamma r^*)$$
$$+ \frac{(1 - \gamma r^*)^2}{\gamma^2}\ln(1 + \gamma - \gamma r^*), \quad 0 \le r^* \le 1, \tag{14}$$

where r^* is defined by Eq. (12).

For h = 0 ($r^* = 1$) this expression is identical to Eq. (10).

An expansion of Eq. (14) for small $\gamma \lesssim 1$, which is useful for practical calculations, has the following form:

$$\mathscr{M}_f = \frac{1}{3}\gamma - \frac{1}{12}\gamma^2\{2(r^*)^4 - 4r^* + 3\} +$$
$$+ \frac{1}{30}\gamma^3\{10(r^*)^2 - 15r^* + 6\}, \quad \gamma \le 1. \tag{15}$$

On further decrease of the field $h \le -\ln(1 + \gamma)$ the sign of the field over the entire sample volume becomes negative (Figs. 4 and 5, case g) and we return to the already studied case shown in Figs. 4 and 5, case b. The corresponding value for the magnetic moment can be written down immediately, changing the signs in front of $\mathscr{M}$ and h in Eq. (9)[8]:

$$\mathscr{M}_g = \frac{3}{2} - \frac{1}{\gamma} e^{-h} - \frac{1}{\gamma^2}(\gamma - e^{-h})^2 \ln(1 - \gamma e^h). \tag{16}$$

Similarly, the portion of the magnetization curve in the fourth quadrant (M < 0, $H_0 < 0$) is obtained from Eq. (9) by changing the signs in front of M and h. Thus, the complete hysteresis loop is symmetric relative to inversion at the origin of coordinates M = H_0 = 0.

It is also easy to generalize the magnetic moment calculation to the case of partial hysteresis cycles. Let us consider, for example, the case in which the transition from portion b of the magnetization curve to portion d begins at some finite value of the external field H_0^* and occurs along curve c (see Fig. 4). The field distribution in this case is shown in Fig. 5, case c. On reduction of the magnetic field (H < H_0^*), cur-

rents are induced in the near-surface zone of the sample which attempt to maintain the value $H > H_0^*$ over the entire region $r^* \leq r \leq 1$. In this region a paramagnetic state exists which can be described Eq. (6). The solution is given by Eq. (7).

In the central part of the sample a diamagnetic state is preserved which is described by Eq. (5) with the boundary condition $h(r^*) = h_0^* = H_0^*/H_{cr}$. The field in the central part of the sample varies according to a law

$$H = H_{cr} \ln [\exp (h_0^*) - \gamma (r^* - r)]. \tag{17}$$

From the condition of continuity of solutions (7) and (17) at $r = r^*$ we find the relation

$$\exp(h_0^*) = \exp(h_0) + \gamma(1 - r^*). \tag{18}$$

By means of Eqs. (7), (7), (17), and (18) we find an expression for the magnetic moment:

$$\mathcal{M}_c = -\gamma \int_0^{r^*} \frac{r^2 dr}{\exp(h_0^*) + \gamma(r - r^*)} + \gamma \int_r^1 \frac{r^2 dr}{\exp(h_0^*) - \gamma(r - r^*)}. \tag{19}$$

In exactly the same way we can obtain expressions describing any partial cycle of the magnetization loop.

4. COMPARISON OF EXPERIMENTAL DATA ON M(H) WITH THEORETICAL CALCULATIONS OF THE HYSTERESIS LOOP

Figure 6 shows a measured hysteresis loop in sample No. 55b, which was prepared from Zr-35% Nb alloy. Also shown are the theoretical points for the a and b portions of the loop (Fig. 4).

In Fig. 7 the theoretical function M(H) is compared with experiment for all branches of the hysteresis loop. The measurements were made in sample No. 63 ($\gamma = 0.29$, $H_0(r^*) = 4.6$ kOe), which was prepared from Zr-20% Nb alloy. The calculation was made with Eqs. (12) and (13) from ref. 8 and Eqs. (9), (10), (15), and (16). The values of j_0 and H_{cr} found from measurements of $j_{c\perp}(H)$ are $j_0 = 3.5 \times 10^5$ A/cm^2, $H_{cr} = 18$ kOe.

From the curve of $j_{c\perp}(H)$ plotted on a semilogarithmic scale it follows (see Fig. 7) that the exponential dependence of $j_c(H)$ is retained up to external field values $H_0 \sim 40$ kOe. In this same region agreement is observed between the measured and calculated M(H) values. An exception is the region of the maxima adjacent to zero magnetizing field, where the experimental points lie significantly above the theoretical curve. In comparison of theory with experiment the scale was determined from the slope of the initial portion of the magnetization curve.

In samples No. 55a, b, and c, which were prepared from Zr-35% Nb alloy with subsequent etching, as previously in Ti-22% Nb alloy[8] and in agreement with Eq. (10) from ref. 8, a size effect was observed: as the sample radius was decreased the maxima in the initial magnetization curve and in the hysteresis loop shifted to lower magnetizing fields.

Thus, the experimental dependence of the magnetic moment associated with the induced currents (the irreversible magnetization curve) in alloys with a rigidly pinned vortex lattice agrees with theoretical values for the hysteresis cycle in the range of magnetizing fields $0 < H_0 < 0.5$ H_{c2}, where as a consequence of the ex-
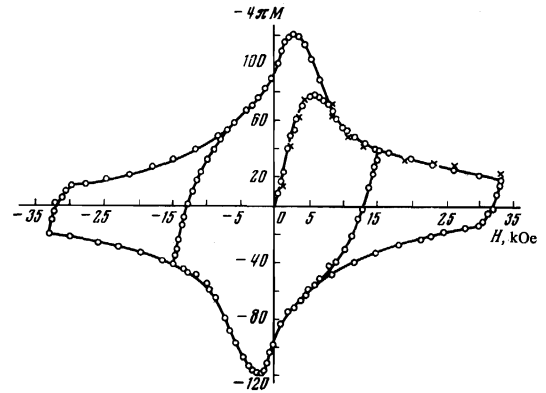

FIG. 6. Comparison of the experimental function M(H) (M in arbitrary units) with equations (12) and (13) of ref. 8. Alloy Zr-35% Nb, sample No. 55b, T = 4.2°K. O—experiment, X—theoretical function $\mathcal{M}(H)$,
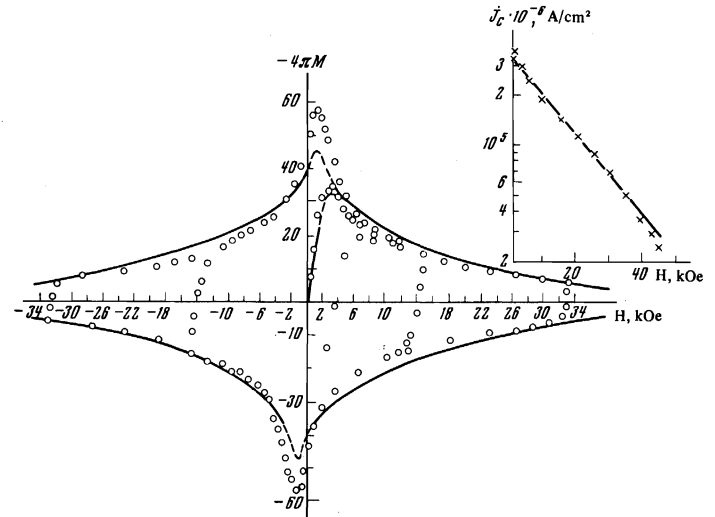

FIG. 7. Dependence of M(H) (M in arbitrary units) and $j_c(H)$ of sample No. 63. Alloy Zr-20% Nb, T = 4.2°K. Points—experiment, solid curve—theoretical dependence of $\mathcal{M}(H)$. At the upper right is shown the function $f_c(H)$ for $j \perp H$; X—experiment.

ponential relation of j_c and H the theoretical formulas have a simple form.

The cause of the discrepancy between theory and experiment near $H_0 = 0$ is still unknown.

CONCLUSION

Study of the dependence of critical current on magnetic field ($j \perp H$) and of the irreversible magnetization curves, carried out in alloys of zirconium with niobium containing disperse particles of the ω phase (Zr-20% Nb) and of the α phase (Zr-35% Nb) has shown that these alloys, like Ti-22% Nb alloys[1], are characterized under certain conditions by a rigid vortex lattice.

Here j_c and H are related by an exponential dependence (2) in the region $0 < H_0 < 0.5$ H_{c2}. The rigid vortex lattice assures the obtaining of critical currents which are limiting for a given material[15]. It arises under annealing conditions such that, as the result of aging of the alloys in the superconducting matrix, there arise nonsuperconducting particles whose size exceeds the core diameter of the Abrikosov vortex[1,8].

In conclusion the authors thank B. M. Vul for his attention to this work and for his valuable advice, I. Yu. Shebalin, G. T. Nikitina, I. A. Baranov, and R. S. Shmulevich for assistance in preparing the samples and carrying out the experiments.

[1] Yu. F. Bychkov, V. G. Vereshchagin, V. R. Karasik, G. B. Kurganov, and V. A. Mal'tsev, Zh. Eksp. Teor. Fiz. **56**, 505 (1969) [Sov. Phys.-JETP **29**, 276 (1969)].

[2] V. D. Borodich, A. P. Golub', A. K. Kombarov, M. G. Kremlev, N. K. Moroz, B. N. Samoĭlov, and V. Ya. Fil'kin, Zh. Eksp. Teor. Fiz. **44**, 110 (1963) [Sov. Phys.-JETP **17**, 76 (1963)].

[3] Yu. F. Bychkov, I. N. Goncharov, M. Litomisskiĭ, V. I. Kuz'min, and I. S. Khukhareva, JINR preprint, No. 1304, Dubna, 1963.

[4] Yu. F. Bychkov, I. N. Goncharov, V. I. Kuz'min, and I. S. Khukhareva, Prib. Tekh. Eksp., 3, 170 (1964).

[5] Yu. F. Bychkov, I. N. Goncharov, and I. S. Khukhareva, Zh. Eksp. Teor. Fiz. **48**, 818 (1965) [Sov. Phys.-JETP **21**, 543 (1965)].

[6] I. A. Baranov, Yu. F. Bychkov, I. N. Goncharov, M. T. Zuev, M. Litomisskiĭ, L. V. Petrova, I. Ruzhichka, V. Ya. Fil'kin, and R. S. Shmulevich, JINR preprint No. 2612, Dubna, 1967.

[7] I. N. Goncharov, Candidate's dissertation, Dubna, 1967.

[8] V. P. Karasik, N G. Vasil'ev, and V. G. Ershov, Zh. Eksp. Teor. Fiz. **59**, 790 (1970) [Sov. Phys.-JETP **32**, 433 (1971)].

[9] Yu. F. Bychkov and M. T. Zuev, Sbornik Metallurgiya i metallovedenie chistykh metallov (Collection on Metallurgy and Processing of Pure Metals) 6, 82 (1967).

[10] K. M. Ralls, R. M. Rose, and J. Wulff, J. Appl. Phys. 36, 1295 (1965).

[11] Yu. F. Bychkov, V. G. Vereshchagin, M. T. Zuev, V. R. Karasik, G. B. Kurganov, and V. A. Mal'tsev, ZhETF Pis. Red. **9**, 451 (1969) [JETP Letters 9, 271 (1969)].

[12] I. N. Goncharov, I. S. Khukhareva, M. Litomisskiĭ, and I. Ruzhichka, Trudy X Mezhdunarodnoĭ konferentsii po fizike nizkikh temperatur (Proceedings X Intern. Conf. on Low Temperature Physics), **2B**, All-Union Institute of Scientific and Technical Information, 1967, p. 70.

[13] C. Baker and J. Sutton, Phil. Mag. 19, 1223 (1969).

[14] C. P. Bean, Phys. Rev. Letters 8, 250 (1962).

[15] V. R. Karasik and V. G. Vereshchagin, Zh. Eksp. Teor. Fiz. 59, 36 (1970) [Sov. Phys.-JETP 32, 20 (1971)].